Hydrogenated amorphous silicon deposited under accurately controlled ion bombardment using pulse-shaped substrate biasing

M. A. Wank,[1,a)] R. A. C. M. M. van Swaaij,[1] P. Kudlacek,[2] M. C. M. van de Sanden,[2] and M. Zeman[1]
[1]*Photovoltaic Materials and Devices Group/DIMES, Delft University of Technology, P.O. Box 5053, Delft 2600 GB, The Netherlands*
[2]*Department of Applied Physics, Plasma and Material Processing Group, Eindhoven University of Technology, Eindhoven 5600 MB, The Netherlands*

(Received 22 June 2010; accepted 27 September 2010; published online 18 November 2010)

We have applied pulse-shaped biasing to the expanding thermal plasma deposition of hydrogenated amorphous silicon at substrate temperatures ~200 °C and growth rates around 1 nm/s. Substrate voltage measurements and measurements with a retarding field energy analyzer demonstrate the achieved control over the ion energy distribution for deposition on conductive substrates and for deposition of conductive materials on nonconductive substrates. Presence of negative ions/particles in the $Ar-H_2-SiH_4$ plasma is deduced from a voltage offset during biasing. Densification of the material at low Urbach energies is observed at a deposited energy <4.8 eV/Si atom and attributed to an increase in surface mobility of mobile species as well as well as surface atom displacement. The subsequent increase in Urbach energy >4.8 eV/Si atom is attributed to bulk atom displacement in subsurface layers. We make the unique experimental observation of a decreasing Tauc band gap at increasing total hydrogen concentration—this allows to directly relate the band gap of amorphous silicon to the presence of nanovoids in the material. © *2010 American Institute of Physics*. [doi:10.1063/1.3505794]

I. INTRODUCTION

Hydrogenated amorphous silicon (a-Si:H) is an increasingly important material for application in devices such as thin film transistors[1] and thin film solar cells.[2] While the most common method for deposition of a-Si:H is parallel-plate radio frequency-plasma enhanced chemical vapor deposition (PECVD), there are numerous other deposition techniques available today, like very high-frequency (VHF) PECVD, hot-wire CVD, or expanding thermal plasma CVD (ETP-CVD) used in this work. Film growth of a-Si:H in ETP-CVD is a result of predominantly SiH_3 radicals forming in the plasma and reacting with the substrate surface,[3] as often observed for plasma-based deposition techniques. All these plasma-based techniques have a complex surface chemistry in common, involving interaction between growth radicals, gas molecules, different types of ions, and the substrate surface itself. The interaction of these reactive species with the surface at given gas pressure and substrate temperature determine the quality of the final bulk film. Understanding these processes is crucial to optimize deposition conditions and obtain the optimal material for the required applications.

While the effect of different gas flows, pressure, substrate temperature, and other parameters are well understood for CVD techniques in general and also for ETP-CVD technique,[4] knowledge about the effect of ion bombardment is still comparatively poor for a-Si:H thin-film growth. In recent studies it was shown that ion bombardment offers additional control over film growth, with promising results demonstrating dense films at deposition conditions usually resulting in void-rich low-density material.[5–13] It is therefore of great technological importance to understand the effect of ion bombardment on a-Si:H film growth, not only for the ETP-CVD technique but for any kind of plasma-involving CVD in general.

The type of interaction between bombarding ion and the a-Si:H film depends mostly on the amount of energy transferred from impinging ions to substrate surface or, at higher energies, subsurface layers. Important parameters to determine the type of interaction are the ion energy, ion flux, the mass ratio between bombarding ion and the target atom, the ion/atom arrival ratio and the average energy provided by ions per deposited Si atom. Achieving control over these parameters is crucial in order to systematically study ion-surface interaction. Control over all three parameters is given in a secondary ion source like, e.g., an ion gun, which gives control over ion flux, ion energy, and the type of ion created. Drawbacks of ion guns are their limitation to lower ion currents and low pressures for operation as well as their higher cost. In the approach discussed in this paper, a secondary ion source is not required and only the ions naturally present in the plasma are accelerated toward the substrate surface, excluding the risk of disturbing the plasma chemistry by the energetic secondary ions. Utilizing a special type of substrate biasing, called pulse-shaped biasing (PSB), control over the ion-energy distribution function (IEDF) is obtained,[14] resulting in a narrow distribution with a distribution peak that can be scanned over a wide range of energies, in our case up to 200 eV. With control over the IEDF, we are able to attribute changes in material properties to specific ion—surface atom and ion—bulk atom interactions. The PSB has only minor

[a)]Electronic mail: m.a.wank@dimes.tudelft.nl.

 © 2010 American Institute of Physics

Downloaded 20 Dec 2010 to 131.180.130.114. Redistribution subject to AIP license or copyright; see http://jap.aip.org/about/rights_and_permissions

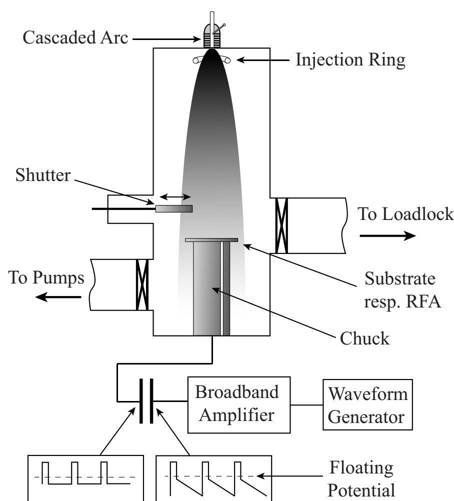

FIG. 1. Schematic drawing of the ETP-CVD setup and the connected PSB setup.

effects on the plasma chemistry[6] and thus in addition to the common processing parameters (e.g., substrate temperature, gas flows) two additional, independent parameters are obtained: the average energy of ions determined by the substrate voltage, as well as the ion current determined by the shape of the wave form.

This article is organized as follows. In the experimental section we describe briefly the ETP-CVD technique and the pulse-shape biasing. We then present the results, which is split into two parts. In the first part we will demonstrate the principle of PSB. We will show how PSB results in a narrow and controllable IEDF, and how different types of substrates can result in the loss of this control if not addressed properly. In the second part we will show results of a-Si:H thin films deposited with PSB. We will discuss the results in terms of ion—thin film interaction and determine an energy range for bombarding ions ideal to obtain dense and void-free a-Si:H deposition.

II. EXPERIMENTAL

The deposition method used in this work, the ETP-CVD technique, is a remote plasma technique. A schematic representation is shown in Fig. 1. The technique has been described in detail elsewhere.[4] In brief, an $Ar-H_2$ plasma is ignited and sustained in a cascaded arc at pressures around 0.46 bar. The plasma expands supersonically through a nozzle into a low pressure deposition chamber ($\sim$0.14 mbar). The nozzle also serves as an additional injection point for H_2 gas. The SiH_4 gas is injected into the $Ar-H_2$ plasma through an injection ring $\sim$10 cm below the nozzle and subsequently dissociates predominantly into SiH_3. These radicals are transported to the temperature controlled substrate holder where the a-Si:H film is deposited.

For all depositions the gas flows were 570 SCCM (SCCM denotes cubic centimeter per minute at STP) Ar and 190 SCCM H_2 in the arc, 150 SCCM H_2 in the nozzle, and 230 SCCM SiH_4 in the injection ring, at a current of 40 A in the arc. Due to interference between the applied voltage and the thermocouple located in the chuck the thermocouple had to be disconnected during biased depositions, impeding active temperature control during depositions. To accommodate for this restriction, the samples were heated up to 210 °C prior to deposition before the thermocouple was disconnected. During deposition the sample cooled down to about 185 °C. Deposition time was 6.15 min for all depositions. The deposition rate was about 0.8 nm/s for unbiased and up to 1 nm/s for biased depositions.

For a remote plasma like the ETP, ions are accelerated to the substrate only by the induced substrate self-bias, for the ETP typically <2 V.[4] Without substrate biasing this leads to negligible ion energy compared to the applied voltages of up to 200 V in this study. Therefore the ETP-CVD technique is a very suitable system to study the effect of controlled ion bombardment on film growth.

The PSB setup has been designed similar to the setup described by Wang and Wendt[14] and has been adapted to our ETP reactor. The whole setup can be seen in Fig. 1. The nonsinusoidal wave form is created by an arbitrary waveform generator (Agilent 33250A) and a broadband amplifier (Amplifier Research 150A250) with an amplification range from 10 kHz up to 250 MHz. The amplifier is connected via a 1 nF blocking capacitor to the chuck where either the substrate holder or the retarding field energy analyzer (RFEA) unit are located. In principle, this setup enables us to operate in a frequency range for the nonsinusoidal wave from 10 kHz up to 8 MHz, but in this work a frequency of 100 kHz was used for all depositions, resulting in a period of 10 μs, unless noted otherwise.

The general idea of PSB is that by coupling a specially tailored wave form to the substrate via a blocking capacitor, a constant negative potential can be obtained on the sample holder for most part of one period, T, of the wave form. This results in a very narrow IEDF contrary to the broad and bimodal IEDF obtained with rf biasing,[14] assuming the sheath transit time is much shorter than the duration of the period with constant potential.[15] A schematic version of the waveform at the amplifier output can be seen in Fig. 2(a) and on the substrate surface in Fig. 2(b). Each period of the amplifier output consists of a ramp with a negative slope followed by a discharge pulse. During the ramp part of the waveform, positive charge carriers are accelerated toward the substrate holder due to the potential difference, and charge is accumulated on the substrate holder due to the blocking capacitor. The negative slope, V_{slope}, in the output signal of the amplifier is tuned in such a way that it exactly balances this charge built-up. As a result we obtain a constant negative potential V_{front} on the substrate surface during the ramp. The pulses are necessary to discharge this built-up charge regularly, allowing negative charge carriers to reach the substrate surface, which occurs at voltages above the floating potential, for ETP technique around >-2 V as explained above. The result is a constant negative potential between the discharge pulses. Important features in this waveform are the potential drop during the ramp, V_{slope}, the duration of the ramp, t_{ramp}, the potential during the discharge pulse, V_{pulse}, the duration of the pulse, t_{pulse}, and the average negative potential obtained during the ramp on the substrate surface. This last parameter has been measured in two ways: indi-

Downloaded 20 Dec 2010 to 131.180.130.114. Redistribution subject to AIP license or copyright; see http://jap.aip.org/about/rights_and_permissions

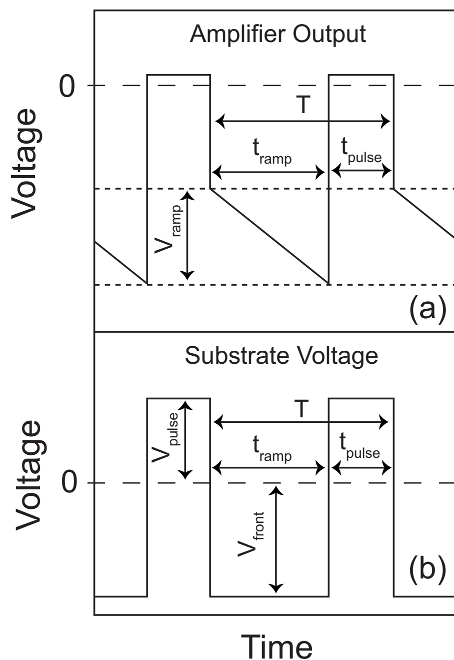

FIG. 2. Schematic versions of the applied pulse-shaped wave form (a) at the broadband amplifier output and (b) on the substrate surface. Important characteristics of the wave forms are indicated in the figure.

rectly by means of a voltage probe on the substrate side of the blocking capacitor (V_{aC}), or directly on the substrate surface, in our case with a Tektronix 1/100 passive voltage probe (V_{front}). Ideally these two voltages are identical, but for a nonconductive substrate they can be significantly different, as will be discussed below. In the following, we will use the term V_{front} in general, and only distinguish between these two methods where required. As V_{front} is much larger than the plasma potential, V_{front} determines the average energy of the ions entering the sheath region. In all our experiments with a period of $T=10$ μs the duration of pulse and ramp were $t_{pulse}=2.5$ μs and $t_{ramp}=7.5$ μs, respectively. The ratio between t_{pulse} and t_{ramp} allows controlling the substrate current, however in this work the ratio was constant for all depositions. The substrate current J_s during the ramp was measured by means of a square tungsten probe, which was placed on the substrate holder and scanned in the voltage range from 0 to -200 V. For more details on the voltage and current measurement we refer to Ref. 16. It should be noted that a weak secondary plasma was visible around the substrate holder during biased depositions.

Time-averaged measurements of the IEDF have been carried out with a commercial planar gridded RFEA (Semion System). More information on the RFEA can be found in Refs. 16 and 17. As the measurement range of the RFEA unit is limited to 150 V, IEDF measurements were limited to $V_{front} < 100$ V to ensure that the whole width of the IEDF peaks can be acquired.

The a-Si:H thin films have been deposited on c-Si wafers (prime wafer, 500–550 μm) with $\sim$2 nm native oxide for *in situ* real-time spectroscopic ellipsometry (RTSE) measurements and Fourier transform infrared spectroscopy (FTIR) analysis (Nicolet 5700, Thermo Electron Corp.). From FTIR spectra the integrated absorption of the wagging mode (at 640 cm^{-1}), the low stretching mode (LSM at 2000 cm^{-1}) and high stretching mode (HSM at 2100 cm^{-1}) have been determined, from which the total hydrogen concentration, c_H, the hydrogen concentration incorporated in vacancies, c_{LSM}, and nanovoids, c_{HSM}, respectively, is calculated. Our *in situ* RTSE measurements were performed using a J. A. Woollam Co., Inc. M-2000F spectroscopic ellipsometer. In our RTSE data analysis we follow a procedure that was described in detail by Van den Oever *et al.*[18] The actual data obtained in an RTSE measurement is the change of the polarization state of the incident light beam, defined by the ellipsometric angles Ψ and Δ, as a function of wavelength. Actual physical information like film thickness and surface roughness are obtained after fitting the ellipsometric angles, in our case with EASE 2.13 software by J. A. Woollam Co. The a-Si:H dielectric function is obtained from the Tauc–Lorentz parameterization. The only dynamic fitting parameters are the bulk film thickness d_b and the surface roughness d_s.

For optical measurements samples were deposited on Corning 7059 glass with coplanar Al contacts to determine optical constants, band gap, and Urbach energy. For reflection-transmission measurements our spectrometer setup consisted of a halogen lamp and a SPEX 1680B monochromator. The Urbach energy was determined from combined reflection-transmission measurements and dual-beam photoconductivity measurements.

It is worth noting that for $V_{front} > 180$ V several samples showed peeling from the substrate surface for both glass and silicon wafers. This indicates significant stress induced at these voltages, e.g., due to thermal gradients induced by local surface heating from ion bombardment, or incorporation of Ar ions into the film.[19]

III. RESULTS AND DISCUSSION

A. PSB analysis

As explained above, the voltage on the substrate surface has been measured in two different ways: directly on the substrate surface (V_{front}) and on the substrate side of the blocking capacitor (V_{aC}). Both are plotted along with the output of the broadband amplifier (V_{bC}) for different substrates in Fig. 3. Three different types of substrates have been used: conductive substrate (a), nonconductive substrate (b), and nonconductive substrate with TCO layer (c). In this case the plasma was a nondepositing $Ar-H_2$ plasma with 710 SCCM Ar and 190 SCCM H_2 in the arc and 150 SCCM H_2 in the nozzle. This type of plasma has a higher substrate current J_s compared to a depositing $Ar-H_2-SiH_4$ plasma as a result of the higher ion density in this type of plasma.[20] Due to faster charging of the substrate under these conditions, a frequency of 125 kHz was required to maintain a flat V_{front} during measurements (alternatively V_{ramp} could have been increased). For a conductive substrate in Fig. 3(a), we clearly see the ramp in the output of the amplifier, V_{bC}, and the resulting flat potential between pulses for both V_{front} and V_{aC}. The overlap between V_{front} and V_{aC} demonstrates that for a conductive substrate V_{aC} accurately represents the potential on the substrate surface. This allows measuring the substrate voltage outside of the deposition reactor and directly on the

Downloaded 20 Dec 2010 to 131.180.130.114. Redistribution subject to AIP license or copyright; see http://jap.aip.org/about/rights_and_permissions

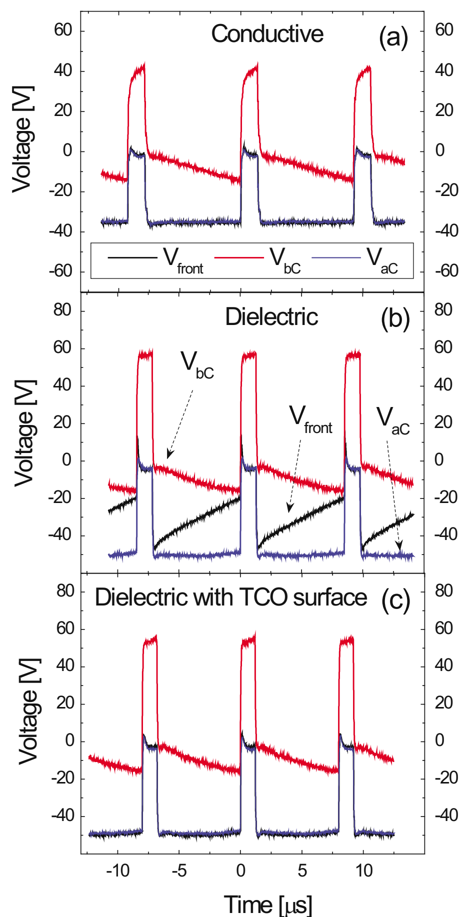

FIG. 3. (Color online) Measured voltages during PSB deposition in an Ar–H_2 plasma on the substrate surface (V_{front}), on the amplifier side of the blocking capacitor (V_{bC}) and on the substrate side of the blocking capacitor (V_{aC}). All three voltages are shown for (a) conductive substrate, (b) nonconductive substrate, and (c) nonconductive substrate with a thin, conductive TCO surface layer.

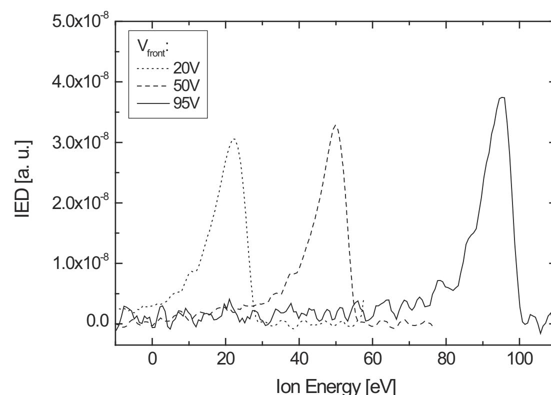

FIG. 4. Ion energy distribution measurements for surface voltages of 20 V (dotted line), 50 V (dashed line), and 95 V (solid line).

blocking capacitor, without the need to have a voltage probe on the substrate surface during deposition. For a nonconductive substrate, however, V_{aC} is clearly different from V_{front} as can be seen in Fig. 3(b). The nonconductive substrate acts as a separate capacitor on the floating chuck, leading to a stronger charge built-up on the substrate surface than on the rest of the substrate holder. Consequently, while V_{aC} measures the whole voltage drop over chuck and substrate surface and appears to be flat during the ramp, the surface potential actually behaves quite different. V_{front} clearly shows a positive slope between the pulses, which is a result of the faster charge built-up on the surface. The constant increase in V_{front} will lead to a much broader IEDF.[16] In case of a nonconductive substrate, V_{aC} can thus not always be used to tune the output waveform and a voltage probe must be used. However, if we have a conductive film on the substrate surface (in this case TCO), we return to the situation of a conductive substrate, as can be seen in Fig. 3(c). In this case the substrate surface was connected to the chuck through the same electrically conductive clamps and screws that are commonly used in this setup. In this setup V_{aC} represents V_{front} accurately again and the two curves overlap so well that they can hardly be distinguished in the figure. We have demonstrated that the presence of a nonconductive substrate is only problematic if a dielectric material is deposited. For the deposition of a conductive material, e.g., a-Si:H in our case, V_{aC} is inaccurate only in the initial phase of the deposition, but will give a very good representation of V_{front} as soon as a closed conductive film is formed. Ion bombardment will thus be accurately controlled for the bulk of the film deposition.

Measurements of the ion energy distribution function can be seen in Fig. 4 for three different substrate voltages V_{front}: 20, 50, and 95 V. The peak position corresponds well to the applied voltage for all three measurements, demonstrating the control achieved over the IEDF. We observe broadening of the peaks which can be split up into two components: a broadening symmetric around the peak position and an additional shoulder at the low-energy side of the peaks. The symmetric broadening around the peak center shows an FWHM of about 6.9 eV, 6.6 eV, and 6.2 eV for 20 V, 50 V, and 95 V, respectively. The FWHM was determined on the high-energy side of the peak and then doubled, to avoid an overestimation due to the low-energy shoulder. This symmetric broadening is a result of noise in the broadband amplifier output signal, which leads to small, continuous variations in the voltage during the ramp. The importance of waveform instabilities for IEDF broadening is discussed in detail in Ref. 16. The additional low-energy shoulder is a result of collisions of ions in the sheath region, leading to scattering losses. Following the collisionless Child law,[21] an increase in substrate voltage leads to an increase in sheath thickness, s. The mean free path, λ_{mfp}, is independent of the substrate voltage, consequently the number of average collision events per ion, s/λ_{mfp}, increases, resulting in an increase in scattering loss with increasing V_{front} and thus a broader low energy shoulder.[22]

In Fig. 5 V_{front} is shown for a conductive substrate in an Ar–H_2–SiH_4 plasma. While in the Ar–H_2 plasma V_{pulse} was only slightly above the floating potential, here V_{pulse} exceeds 100 V. This is related to the current balance that automatically establishes in the system as a result of the blocking capacitor. In general the built-up of charge due to the current of positive charge carriers during the ramp is exactly balanced by the current of negative charge carriers during the pulse. In case of an Ar–H_2 plasma the dominant positive ion is H_3^+ ions[23] and during the pulse free electrons are the

Downloaded 20 Dec 2010 to 131.180.130.114. Redistribution subject to AIP license or copyright; see http://jap.aip.org/about/rights_and_permissions

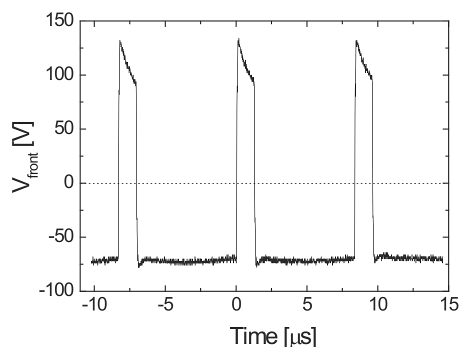

FIG. 5. Measurement of V_{front} for an $Ar-H_2-SiH_4$ plasma, the dotted line marks the 0 V—potential.

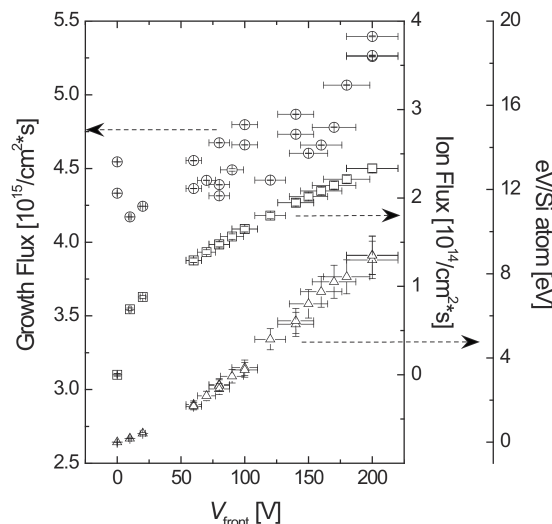

FIG. 6. Growth flux Γ_{Si}, ion flux Γ_{Ion} and energy deposited per incorporated Si atom vs the surface voltage V_{front}.

dominant charge carriers. In both cases the current is a function of the density of the charge carrier, its respective mobility and the potential difference between plasma and substrate. Due to the much higher mobility of the electrons compared to ions, and assuming a similar carrier density, the short pulse duration at a voltage just above the floating potential is sufficient to compensate completely for the charge built-up during the ramp.[24] In case of an $Ar-H_2-SiH_4$ plasma, the pulse voltage of around 100 V suggests a change in composition of negative species in the plasma with lower mobility and lower concentration. This indicates the strong presence of negatively charged ions or particles in the plasma, with a much lower mobility compared to free electrons. In order to maintain a balance between the two currents a voltage offset occurs, leading to the large positive voltage during the pulse, which is necessary to get sufficient negative ions to the substrate surface to fully compensate for the charge on the substrate built-up during the ramp.

A substantial presence of negative ions/particles in the plasma also has an effect on the IEDF using different biasing techniques like rf biasing. Since a considerable part of the voltage would be positive, alternating bombardment with positively and negatively charged ions would occur, instead of the expected bombardment with predominantly positive ions. Furthermore the presence of negative ions/particles leads to a much higher rf power required to obtain the same average substrate voltage V_{dc} as compared to conditions without negative ions/particles in the plasma, which will also result in a much broader IEDF. In case of heavier molecules or dust particles the impact on the substrate surface could result in their break-up. To avoid the large positive voltage during the ramp, the duration t_{pulse} can be increased, giving negative species more time to discharge the substrate during the pulse. Alternatively PSB could be adjusted to achieve control also about the bombardment with negative ions on the substrate surface. Introducing a slope to the pulse similar to the slope of the ramp during negative voltages would allow gaining control also over the energy of negative ions. Ideally this could be used twofold: to break up larger negative ionic clusters upon impact on the surface during the pulse, and to provide the surface with additional energy from controlled ion bombardment during the ramp.

Figure 6 shows the growth flux, the ion flux, and the resulting average energy deposited per incorporated Si atom, electron-volt/Si atom, as a function of substrate voltage. The Clausius–Mossotti relation was used to determine the mass density $\rho_{a\text{-}Si:H}$ of the films from the infrared (IR) refractive index and the total hydrogen content c_H.[25] From the mass density, the growth flux Γ_{Si} could be determined. The ion flux during the ramp Γ_{ion} was directly determined from the substrate current J_s by means of a square tungsten probe. Both fluxes continuously increase with V_{front}. For the growth flux this indicates substrate biasing has a clear effect on the gas phase, leading to additional SiH_3 production in the plasma. An increase in SiH_3 production has been observed in previous studies for rf biasing[5,26] and attributed to additional gas-phase reactions in the secondary plasma around the substrate holder. It was not observed in a recent study on PSB by Martin *et al.*,[6] however, they assumed a constant mass density of 2.25 g/cm^3 and constant IR refractive index for all samples, while we include changes in both mass density and IR refractive index in our analysis via the Clausius–Mossotti relation. The increase in growth flux could also be partly related to the presence of negatively charged ions, as shown above. During biased deposition the large positive voltage during the discharge pulse could lead to their partial break-up and subsequent incorporation into the film. The increase in ion flux is related to both the ionization in the secondary plasma as well as the increase in ion current with increasing V_{front} due to an increase in sheath thickness s and thus collection area around the substrate holder as mentioned above.[27]

The ratio between the two fluxes times the average substrate voltage determines the average energy deposited per incorporated Si atom. Also for the average deposited energy we observe an increase with increasing V_{front}, which is a result of the stronger increase in Γ_{ion} compared to Γ_{Si} (~160% relative increase in Γ_{ion} compared to ~25% for Γ_{Si}, respectively). The following discussion of material properties below will be in terms of deposited energy per Si atom for an easier comparison with results published in literature. It should be noted that the error for the substrate voltage given in Fig. 6 overestimates the actual voltage noise during

Downloaded 20 Dec 2010 to 131.180.130.114. Redistribution subject to AIP license or copyright; see http://jap.aip.org/about/rights_and_permissions

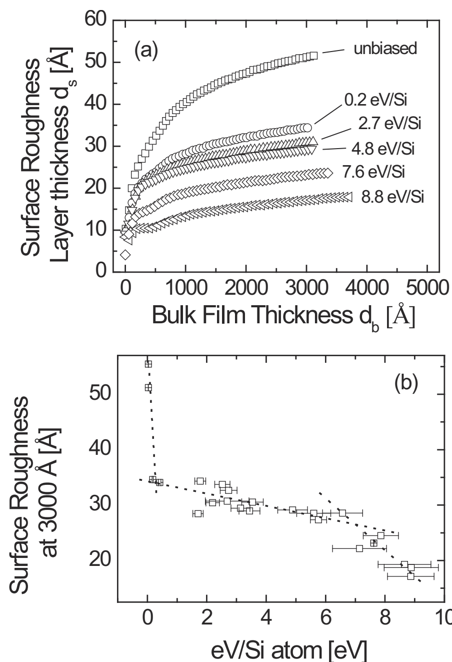

FIG. 7. (a) The surface roughness layer thickness d_s as a function of the bulk film thickness d_b for different deposited energies per Si atom. (b) The surface roughness layer thickness d_s at a bulk film thickness of 3000 Å vs the energy deposited per Si atom.

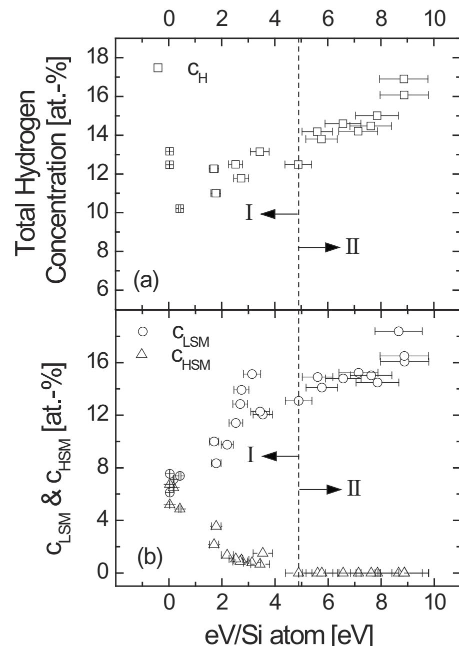

FIG. 8. (a) The total hydrogen concentration c_H as a function of energy deposited per Si atom. (b) The hydrogen associated to divacancies (c_{LSM}) and nanovoids (c_{HSM}) as a function of deposited energy per Si atom. The dashed lines in both figures indicate the transition from region I to region II at 4.8 eV/Si atom.

the ramp. The step size of the volt meter increases with the measured voltage range, resulting in a decreasing resolution. This also leads to an overestimation in the error of the deposited energy.

B. Material analysis

The predominant part of the energy deposited during ion bombardment remains in the surface layer of the film, as the stopping power for Ar ions bombarding on a silicon surface is around 270 eV/nm.[28] We therefore examine the development of the surface roughness d_s versus bulk film thickness d_b, as determined from *in situ* SE as a function of the deposited energy up to 9 eV/Si atom. The surface roughness development as a function of bulk-layer thickness is shown in Fig. 7(a). The roughest films are obtained for unbiased depositions with a surface roughness layer thickness of about 50 Å at 3000 Å bulk film thickness. A strong reduction in d_s is observed already upon mild ion bombardment around 0.2 eV/Si; a further increase in V_{front} leads to even smoother surfaces. At 8.8 eV/Si atom very smooth films below 20 Å d_s are grown, otherwise typically obtained in our ETP-CVD reactor only at growth rates around 1 Å/s or at higher substrate temperatures.[29] Since all depositions had the same deposition time of 6.15 min we can also observe the increase in deposition rate above 4.8 eV/Si atom, which can be concluded from the increase in final bulk film thickness. The surface roughness at 3000 Å bulk film thickness as a function of deposited energy per Si atom can be seen in Fig. 7(b). Three different regions can be distinguished. Already at very low deposited energies <1 eV/Si atom d_s at 3000 Å strongly decreases with substrate voltage. The decrease in d_s between 1 and 4.8 eV/Si atom is much weaker, and becomes larger above 4.8 eV/Si atom. The three areas are indicated in the plot by dotted lines. From the roughness layer development it is clear that an increase in deposited energy leads to smoother surfaces.

FTIR results can be seen in Figs. 8(a) and 8(b). Figure 8(a) shows the dependence of the total hydrogen concentration c_H and Fig. 8(b) the dependence of the LSM mode associated with divacancies, c_{LSM}, and HSM mode associated with nanovoids, c_{HSM}, on the deposited energy per Si atom. The data in Fig. 8(a) show some scattering, but in general the hydrogen concentration increases continuously with electron-volt/Si atom. For <2 eV/Si atom c_H seems to initially decrease, but data in this deposited energy range are sparse. The same continuous increase with increasing energy per deposited Si atom can be observed in Fig. 8(b) for divacancies. The increase appears to be stronger for voltages <4.8 eV/Si atom and weaker for >4.8 eV/Si atom. The absorption due to nanovoids (HSM) continuously decreases until for >4.8 eV/Si atom it could not be determined anymore. This important transition voltage has been marked in Fig. 8(b) with a dashed line and the regions below and above 4.8 eV/Si atom are labeled region I and II, respectively.

The IR refractive index as a function of electron-volt/Si atom is shown in Fig. 9(a) and shows a similar separation into two regions. Below 4.8 eV/Si atom in region I the refractive index continuously increases, indicating an increase in material density. This is in good agreement with the reduction in void content deduced from c_{HSM} in Fig. 8(b). In region II (>4.8 eV/Si atom) the refractive index is constant and does not change with deposited energy, which is also in agreement with the constant c_{HSM} in region II. The clear relation between void concentration and IR refractive index indicates that for our experimental conditions the material

Downloaded 20 Dec 2010 to 131.180.130.114. Redistribution subject to AIP license or copyright; see http://jap.aip.org/about/rights_and_permissions

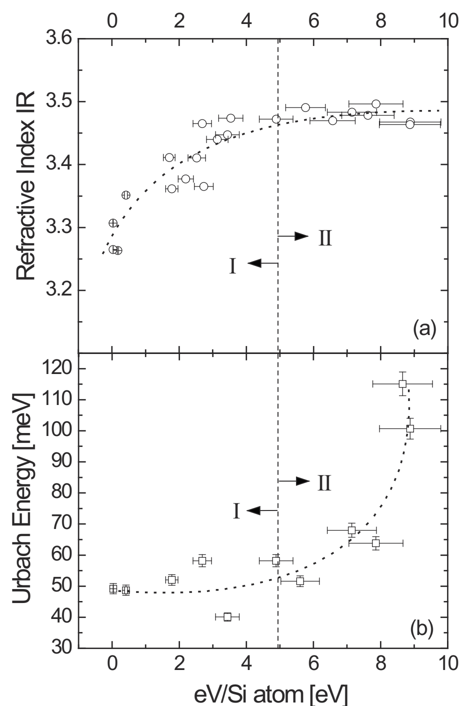

FIG. 9. (a) The refractive index in the infrared as obtained from FTIR analysis vs the deposited energy per Si atom. (b) The Urbach energy vs the deposited energy per Si atom. The dashed lines indicate the transition from region I to region II at 4.8 eV/Si atom, the dotted line in (b) is a guide to the eye.

density mainly depends on the void concentration. No material densification occurs due to a densification of the amorphous matrix upon ion bombardment. The Urbach energy, a good measure for the material disorder, is shown in Fig. 9(b) as a function of energy per deposited Si atom. Low values of around 50 meV are observed for the Urbach energy in region I and an increase can be seen from 4.8 eV/Si atom onwards, with an increasingly sharp raise toward 8 eV/Si atom up to >100 meV indicating incorporation of defects.

The increase in c_H suggests that ion bombardment and substrate temperature are not interchangeable ways of providing the film with energy. Although many film characteristics like film density, surface roughness or nanovoid concentration behave similar for both methods, we observe a clear difference in the variation in c_H HH In our experiments c_H increases with increasing deposited energy, whereas an increase in substrate temperature typically leads to a decrease in c_H.[30]

As seen above, our results can be categorized into two regions, above and below 4.8 eV/Si atom. In region I, for which the deposited energy <4.8 eV/Si atom, we observe a reduction in void content, as concluded from FTIR data in Fig. 8(b), and an increase in material density as concluded from the increase in refractive index in Fig. 9(a). Also the roughness layer thickness development at 3000 Å shown in Fig. 7(b) suggests such a transition region, where surface smoothening is present throughout the deposited energy range, but seems to be enhanced in region II. These observations will be discussed in terms of ion-surface interactions. We assume the dominant ion to be SiH_3^+ as a result of a charge exchange reaction between Ar^+ or H^+ and a SiH_4 molecule.[4,31] Since the mass of the SiH_3^+ ion is very close to the mass of a silicon atom on the film surface the energy transfer between them is very efficient.[28]

At the lowest substrate voltages simple energy transfer from impinging ions to surface atoms results in local thermal spikes and no surface or bulk Si atom displacement occurs yet. The observed smoothening of the surface already at very low energies is possibly related to enhanced surface mobility on the substrate surface, as only these processes can be activated at such low energies.[5] The mobile species are not necessarily SiH_3 radicals, also H atoms or dangling bonds are possible candidates. The threshold energy for surface atom displacement of a Si surface atom exposed to an Ar ion beam (which has a mass close to that of an SiH_3^+ ion, thus we expect a similar energy transfer) has been estimated to be around 18 eV, and the threshold energy for bulk atom displacement around 40 eV.[32] Bulk atom displacement has been shown to increase sharply with increasing ion energy[32] and more energy is deposited in subsurface layers then in the surface layer at ion energies >100 eV. This is due to repeated collisions of ions with atoms in the material at higher energies, with most of the collisions resulting only in a fractional energy transfer from ion to atom. Although sputtering can already occur at 50 eV Ar^+ ion bombardment, it is expected to become relevant for energies >100 eV.[33]

Local thermal spikes and surface atom displacement are sufficient to lead to a strong decrease in surface roughness d_s and an increase in material density as seen from the IR refractive index, without increasing the Urbach energy significantly. Broken bonds created by surface atom displacement can be annihilated easily by the incoming growth flux particles and thus do not contribute to defect creation in the material. On the other hand, in subsurface layers the more rigid atomic structure in the bulk requires more energy to rearrange and defect annihilation is less likely to occur. Thus bulk atom displacement is the most probable effect that leads to defect creation and increased disorder in the material, as can be seen in our Urbach energy data with a strong increase at deposited energies >4.8 eV/Si atom. This energy corresponds to V_{front} of around 100 V, or ion energy of 100 eV which we attribute to the aforementioned mechanism of subsurface atom displacement. The increase in defect density has been observed for RF substrate biasing before.[34] Significant penetration depth for ions at higher energies can also lead to an increase in growth flux, assuming the dominant ion is SiH_3^+. Ions are typically neutralized a few angstroms above the substrate surface via a charge-exchange mechanism (Auger or resonant tunneling process).[35] Thus the substrate surface is in fact bombarded by neutral radicals, but with the energy of the previously neutralized ion. While SiH_3 radicals typically have a reaction coefficient of 0.3 on an a-Si:H surface,[26] the penetration of the bombarding radicals deeper into the film at sufficient energies can lead to a sticking coefficient on the order of 1, as suggested by Hamers *et al.*[7] This effect might in fact be visible in Fig. 6 where the growth flux appears to be increasing stronger above 150 V, or equivalently >4.8 eV/Si atom deposited. The enhanced smoothening at ion energies >4.8 eV/Si atom observed in

Downloaded 20 Dec 2010 to 131.180.130.114. Redistribution subject to AIP license or copyright; see http://jap.aip.org/about/rights_and_permissions

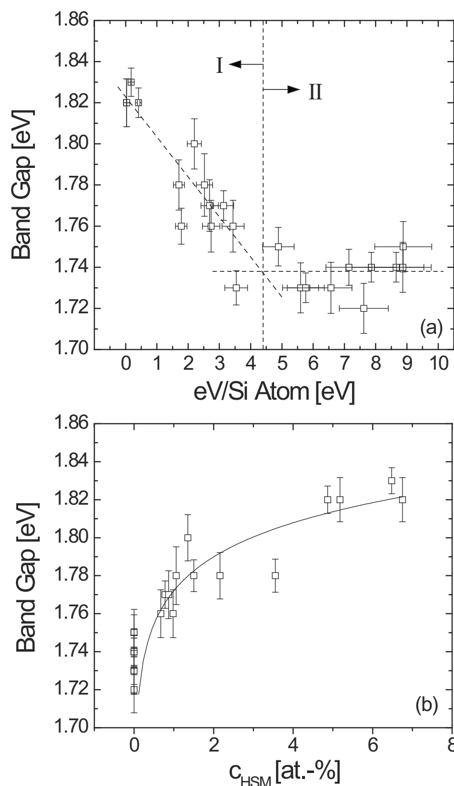

FIG. 10. (a) The Tauc band gap as a function of deposited energy per Si atom. The vertical dashed line indicates the transition from region I to region II at 4.8 eV/Si atom, the other dashed lines are guides to the eye. (b) The Tauc band gap vs the concentration of hydrogen associated to nanovoids, c_{HSM}. The solid line is a guide to the eye.

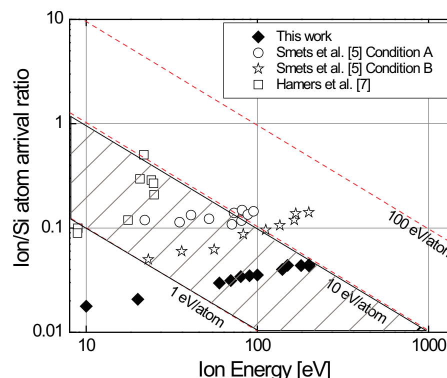

FIG. 11. (Color online) Energy deposition map containing results from this work (full diamonds), two experimental conditions of Smets *et al.* (empty circles and empty stars) and Hamers *et al.*(empty squares). The shaded area marks the region considered useful for film densification during ion-assisted film-deposition by Kaufman *et al.* (Ref. 34).

Fig. 7(b) can be related to enhanced etching or sputtering of the surface, which starts to become significant for V_{front} >100 V.

While the increase in divacancy density for energies <4.8 eV/Si atom could be a result of the decrease in void concentration and their transformation into vacancies, we attribute the increasing divacancy density for energies >4.8 eV/Si atom to the breaking of subsurface bonds due to bulk atom displacement and subsequent saturation of the created dangling bond by a hydrogen atom.[5] We observe strong similarities with results reported on rf substrate biasing[5] for material grown at similar growth rates, whereas we do not observe the increase in nanovoid concentration reported by Smets *et al.*,[5] which were obtained for higher growth rates around 2–4 nm/s and voltages >100 V.

The Tauc band gap as a function of energy per deposited Si atom can be seen in Fig. 10(a). We observe two regions in band gap development with increasing deposited energy. Starting at 1.82 eV for unbiased material the band gap drops to ~1.74 eV at 4.8 eV/Si atom. For deposited energies >4.8 eV/Si atom the band gap is constant around 1.74 eV. Commonly a change in a-Si:H Tauc band gap is related to a change in hydrogen content c_H, usually observing an increase in band gap with increasing c_H.[30] However, comparing Fig. 10(a) with Fig. 8(a), we observe the opposite trend for our data: a *decrease* in band gap with increasing c_H. However, when plotting the Tauc band gap versus the concentration of hydrogen in nanovoids, c_{HSM}, in Fig. 10(b) we see a strong correlation. This observation has been made before by Fukutani *et al.*[36] They concluded from their study on sequential hydrogen and Ar ion treatments that the band gap is most strongly correlated with c_{HSM} whereas c_H, c_{LSM}, and R^* only seem correlated with the band gap through their own correlation with c_{HSM}. In a related publication, Fortmann[37] suggests a phonon band–indirect optical gap model to explain the dependence of the band gap on c_{HSM}. Commonly, parameters that lead to a reduction in the total hydrogen content also lead to a reduction in void concentration in the material (e.g., an increasing substrate temperature), which hides the trend we observed and suggests that the band gap is related to c_H. In this context PSB is unique, as it leads to an increase in c_H while c_{HSM} *decreases*, for the first time experimentally revealing the underlying trend between hydrogen and band gap. We therefore believe that our results strongly suggest the band gap dependence on c_{HSM} described above. Additionally, two distinct slopes can be observed in Fig. 10(b), a steep slope <2 at. % c_{HSM} and a less steep slope >2 at. % c_{HSM}. A similar observation has been made by Smets *et al.*[5] before and it was suggested that the band gap is affected differently by small voids <2 at. % c_{HSM} than by larger voids >2 at. % c_{HSM}.

Following a concept introduced by Kaufman *et al.*,[34] Fig. 11 shows an energy deposition map. The figure contains data from our work along with data from Smets *et al.*[5] deposited with the ETP-CVD technique as well as data from Hamers *et al.*[7] deposited with VHF-PECVD. The results from Smets *et al.*[5] obtained for rf biasing under condition A correspond to a-Si:H films grown at 1.1–1.7 nm/s and under condition B to films grown at 2.5–4.2 nm/s and show densification below 10 eV/Si atom similar to our results. Hamers *et al.*[7] report also material densification for ion energy depositions below <10 eV/atom and constant material density for >10 eV/atom. Harper *et al.*[38] argued that for ion assisted thin-film deposition the range of deposited ion energy that leads to material densification without increase in defect density lies between 1 and 10 eV/atom. This range is indicated in Fig. 5 by the dashed area. Most of our samples fall into this range of deposited energy, samples from region I

Downloaded 20 Dec 2010 to 131.180.130.114. Redistribution subject to AIP license or copyright; see http://jap.aip.org/about/rights_and_permissions

that increase in density while retaining a low Urbach energy as well as samples from region II that show no increase in material density, but instead an increase in Urbach energy and presumably also in defect density. This latter increase suggests that Harpers suggestion about the ideal energy deposition range <10 eV/Si atom is too general. From the average deposited energy alone conclusions about the changes in material properties cannot be drawn. It is necessary to obtain information about the ion energy distribution and subsequently ion—surface- or bulk-atom interactions in order to determine ideal conditions for ion-assisted thin film deposition. We conclude from our results reported here that for ETP-CVD with PSB, the densest material with low defect density is obtained around 5 eV/Si atom.

IV. CONCLUSION

PSB has been investigated as a technique to achieve controlled ion bombardment during a-Si:H deposition with ETP-CVD at substrate temperatures ~ 200 °C. Accurate control over the substrate voltage is achieved for conductive substrates or nonconductive substrates when a conductive surface layer is connected to the substrate holder. Good control over the IEDF has been demonstrated with retarding field analyzer measurements for $V_{\mathrm{front}} < 100$ V. The presence of negative ions/particles in the $Ar-H_2-SiH_4$ plasma is deduced from large positive voltages during the discharge pulse.

For material analysis as function of deposited energy per silicon atom we can distinguish roughly between two regions, region I <4.8 eV/Si atom and region II >4.8 eV/Si atom. Throughout region I we observe an increase in material density due to a decrease in nanovoid concentration as deduced from FTIR analysis. At the transition between region I and II around 4.8 eV/Si atom the densest material with low nanovoid concentration and low Urbach energy is obtained. Above 4.8 eV/Si atom we see an increase in Urbach energy. The increase in material density and the reduction in surface roughness are attributed to an increase in surface mobility of mobile species as well as surface atom displacement. The increase in Urbach energy is related to bulk atom displacement in subsurface layers at higher ion energies. We report a clear dependence of the band gap on hydrogen in nanovoids as determined from the c_{HSM} mode, and not the correlation with the total hydrogen concentration c_{H} which is typically reported in literature. To our knowledge this is a unique experimental observation.

ACKNOWLEDGMENTS

Kasper Zwetsloot, Martijn Tijssen, Stefaan Heirman, and Jan Chris Staalenburg are acknowledged for their skilful technical assistance. Kehinde Adejumo is acknowledged for her help with sample measurements and analysis. This research is part of the Hi-RASE project and was financially supported by SenterNovem within the framework of the EOS-LT program.

[1] Y. Kuo, J. Electrochem. Soc. **142**, 2486 (1995).
[2] L. L. Kazmerski, J. Electron Spectrosc. Relat. Phenom. **150**, 105 (2006).
[3] W. M. M. Kessels, A. H. M. Smets, D. C. Marra, E. S. Aydil, D. C. Schram, and M. C. M. van de Sanden, Thin Solid Films **383**, 154 (2001).
[4] M. C. M. van de Sanden, R. J. Severens, W. M. M. Kessels, R. F. G. Meulenbroeks, and D. C. Schram, J. Appl. Phys. **84**, 2426 (1998).
[5] A. H. M. Smets, W. M. M. Kessels, and M. C. M. van de Sanden, J. Appl. Phys. **102**, 073523 (2007).
[6] I. T. Martin, M. A. Wank, M. A. Blauw, R. A. C. M. M. Van Swaaij, W. M. M. Kessels, and M. C. M. Van de Sanden, Plasma Sources Sci. Technol. **19**, 015012 (2010).
[7] E. A. G. Hamers, W. G. J. H. M. van Sark, J. Bezemer, H. Meiling, and W. F. van der Weg, J. Non-Cryst. Solids **226**, 205 (1998).
[8] B. Drevillon, J. Huc, and N. Boussarssar, J. Non-Cryst. Solids **59–60**, 735 (1983).
[9] T. V. Herak, T. T. Chau, S. R. Mejia, P. K. Shufflebotham, J. J. Schellenberg, H. C. Card, K. C. Kao, and R. D. McLeod, J. Non-Cryst. Solids **97–98**, 277 (1987).
[10] H. Rinnert, M. Vergnat, G. Marchal, and A. Burneau, Nucl. Instrum. Methods Phys. Res. B **147**, 79 (1999).
[11] P. Roca i Cabarrocas, P. Morin, V. Chu, J. P. Conde, J. Z. Liu, H. R. Park, and S. Wagner, J. Appl. Phys. **69**, 2942 (1991).
[12] A. S. Abramov, A. I. Kosarev, P. Roca i Cabarrocas, M. V. Shutov, and A. J. Vinogradov, Thin Solid Films **383**, 178 (2001).
[13] S. Zhang and D. E. Brodie, J. Phys.: Condens. Matter **3**, 6597 (1991).
[14] S. B. Wang and A. E. Wendt, J. Appl. Phys. **88**, 643 (2000).
[15] E. V. Barnat and T. M. Lu, J. Appl. Phys. **92**, 2984 (2002).
[16] P. Kudlacek, R. F. Rumphorst, and M. C. M. van de Sanden, J. Appl. Phys. **106**, 073303 (2009).
[17] D. Gahan, B. Dolinaj, and M. B. Hopkins, Rev. Sci. Instrum. **79**, 033502 (2008).
[18] P. J. van den Oever, M. C. M. van de Sanden, and W. M. M. Kessels, J. Appl. Phys. **101**, 123529 (2007).
[19] S. M. Rossnagel and J. J. Cuomo, Vacuum **38**, 73 (1988).
[20] W. M. M. Kessels, C. M. Leewis, A. Leroux, M. C. M. van de Sanden, and D. C. Schram, J. Vac. Sci. Technol. A **17**, 1531 (1999).
[21] M. A. Lieberman and A. J. Lichtenberg, *Principles of Plasma Discharges and Materials Processing* (Wiley, New York, 1994).
[22] W. D. Davis and T. A. Vanderslice, Phys. Rev. **131**, 219 (1963).
[23] M. C. M. Van De Sanden, M. Van Der Steen, G. J. H. Brussaard, M. Carrére, and D. C. Schram, Surf. Coat. Technol. **98**, 1416 (1998).
[24] B. Chapman, *Glow Discharge Processes: Sputtering and Plasma Etching* (Wiley-Interscience, New York, 1980).
[25] A. H. M. Smets, W. M. M. Kessels, and M. C. M. van de Sanden, Appl. Phys. Lett. **82**, 1547 (2003).
[26] J. P. M. Hoefnagels, Y. Barrell, W. M. M. Kessels, and M. C. M. van de Sanden, J. Appl. Phys. **96**, 4094 (2004).
[27] E. Stamate and H. Sugai, Phys. Rev. E **72**, 036407 (2005).
[28] A. R. Gonzalez-Elipe, F. Yubero, and J. M. Sanz, *Low Energy Ion Assisted Film Growth* (Imperial College Press, London, 2003).
[29] M. A. Wank, R. A. C. M. M. van Swaaij, and M. C. M. van de Sanden, Appl. Phys. Lett. **95**, 021503 (2009).
[30] G. D. Cody, B. Abeles, C. R. Wronski, R. B. Stephens, and B. Brooks, Sol. Cells **2**, 227 (1980).
[31] W. M. M. Kessels, M. C. M. van de Sanden, and D. C. Schram, Appl. Phys. Lett. **72**, 2397 (1998).
[32] Z. Q. Ma, Y. F. Zheng, and B. X. Liu, Phys. Status Solidi A **169**, 239 (1998).
[33] K. Wittmaack, Phys. Rev. B **68**, 235211 (2003).
[34] H. R. Kaufman and J. M. E. Harper, J. Vac. Sci. Technol. A **22**, 221 (2004).
[35] D. Marton, *Low Energy Ion-Surface Interactions* (Wiley, New York, 1994).
[36] K. Fukutani, M. Kanbe, W. Futako, B. Kaplan, T. Kamiya, C. M. Fortmann, and I. Shimizu, *17th International Conference on Amorphous and Microcrystalline Semiconductors—Science and Technology (ICAMS 17)*, Budapest, 25–29 August 1997 (Elsevier Science, Budapest, Hungary, 1997).
[37] C. M. Fortmann, Phys. Rev. Lett. **81**, 3683 (1998).
[38] J. M. E. Harper, J. J. Cuomo, R. J. Gambino, and H. R. Kaufman, *Ion Bombardment Modification of Surfaces: Fundamentals and Applications* (Elsevier Science, Amsterdam, 1984).

Downloaded 20 Dec 2010 to 131.180.130.114. Redistribution subject to AIP license or copyright; see http://jap.aip.org/about/rights_and_permissions